Challenge Journal of
CONCRETE RESEARCH LETTERS

Research Article

Influence of calcium leaching on high-volume fly ash roller compacted concrete

Worachai Ponloa [a,*], Suvimol Sujjavanich [b], Prasert Suwanvitaya [b]

[a] *Department of Civil Engineering, Bangkokthonburi University, 10710 Bangkok, Thailand*
[b] *Department of Civil Engineering, Kasetsart University, 10900 Bangkok, Thailand*

ABSTRACT

Calcium leaching is a chemical deterioration process that adversely affects the performance and service life of concrete structures exposed to water. This study aims to examine calcium leaching in high-volume fly ash roller-compacted concrete (HVFA–RCC) under varying permeation pressures and to clarify the influence of pressure-driven transport on calcium loss, microstructural degradation, porosity development, and compressive strength reduction. Concrete specimens prepared with a mix design representative of RCC dams were used in the experimental program, employing a high-volume fly ash mixture with a fly ash-to-cement ratio of 1.11 by weight. To accelerate calcium leaching, the specimens were subjected to permeation pressures of 4, 6, and 9 bar in an ammonium chloride (NH_4Cl) solution for 28 days. After the leaching procedure, the specimens were evaluated through compressive strength testing and microstructural characterization using X-ray diffraction (XRD), scanning electron microscopy (SEM), and energy-dispersive X-ray spectroscopy (EDS). The results indicate that calcium leaching tends to reduce compressive strength and is accompanied by progressive microstructural degradation, with the severity of deterioration increasing as permeation pressure increases. The incorporation of HVFA helps to reduce calcium loss and limits the associated degradation in both microstructure and mechanical performance. These findings suggest that pressure-driven transport contributes to the acceleration of calcium leaching in RCC, while the use of HVFA enhances resistance to leaching-induced damage, thereby supporting improved durability of RCC dams exposed to sustained hydraulic pressure through the mitigation of long-term degradation processes.

ARTICLE INFO

Article history:
Received – December 2, 2025
Revision requested – December 23, 2025
Revision received – February 7, 2026
Accepted – February 20, 2026

Keywords:
Calcium leaching
High-volume fly ash
Durability
Roller compacted concrete
Permeation pressure

Citation: Ponloa W, Sujjavanich S, Suwanvitaya P (2026). Influence of calcium leaching on high-volume fly ash roller compacted concrete. *Challenge Journal of Concrete Research Letters*, 17(2), 94–108.

1. Introduction

Calcium leaching is a chemical deterioration process that affects the durability and service life of concrete structures exposed to water. Hydraulic structures such as dams remain in long-term contact with water during service. This exposure promotes the dissolution of calcium-bearing hydration products from the cement matrix. The process modifies pore structure and gradually weakens the solid skeleton of concrete. As a result, permeability increases and mechanical properties tend to decrease over time, which raises concerns for the long-term performance of concrete dams (Carde and François 1997; Marchand et al. 2001).

Among cement hydration products, calcium hydroxide plays an important role in strength and durability. It exhibits higher solubility than other hydration phases and shows greater sensitivity to water exposure. Calcium leaching commonly initiates with portlandite dissolution and then progresses to gradual decalcification

* *Corresponding author.* E-mail address: worachai.p@ku.th (W. Ponloa)
ISSN: 2548-0928 / DOI: https://doi.org/10.20528/cjcrl.2026.02.002

of C–S–H. This chemical degradation increases porosity and enhances transport-related properties such as diffusivity and permeability. Previous studies reported that leaching-induced pore structure changes strongly influence calcium transport and damage evolution in cementitious materials (Choi and Yang 2013; Cheng et al. 2013; Zhang et al. 2020).

High-volume fly ash (HVFA) concrete has been widely applied in mass concrete and roller-compacted concrete (RCC) dams. Fly ash reduces portlandite content through pozzolanic reactions and contributes to pore structure refinement, a mechanism also observed in silica-fume-modified cementitious materials, where calcium hydroxide consumption and additional C–S–H formation produce a denser matrix and restrict the ingress of aggressive agents (Al-Safi et al. 2025). These effects may enhance resistance to calcium leaching and associated durability loss. Several studies observed that fly ash can slow calcium depletion and mitigate strength degradation under aggressive exposure conditions. However, the effectiveness of fly ash depends on mixture composition, environmental conditions, and binder chemistry, because its pozzolanic contribution may be limited when portlandite availability in the hydrated matrix is insufficient (Kadhim and Keskin 2024). At suitable replacement levels, fly ash can promote particle packing and additional C–S–H formation, whereas excessive substitution of mineral by-products may increase porosity and reduce mechanical and durability performance despite the beneficial filler and pozzolanic effects observed at suitable proportions (Rozière et al. 2009; Fanghui et al. 2014; Shi et al. 2019; Wang et al. 2021; Turan et al. 2025; Shaheen et al. 2025). Comparable improvements have been reported in concretes containing silica- and calcium-rich waste powders, where suitable replacement levels promoted additional C–S–H formation and reduced water penetration through pore refinement (Mahmud et al. 2025).

In actual RCC dams, water seepage develops under hydraulic pressure gradients along the dam height, while fluctuating reservoir and uplift pressures alter the internal stress and displacement states of gravity dams (Pandimani 2025). Seepage rate and flow velocity vary with elevation and internal pressure. Field observations indicated that calcium concentration in seepage water differs between locations within the dam body. These observations suggest that calcium leaching is not governed by diffusion alone. Pressure-driven percolation and advective transport contribute to leaching progression under in-service conditions (Inmala and Soralump 2010; Liu et al. 2022; Chen et al. 2023). Moreover, cracks exposed to reservoir water may facilitate seepage and create additional transport pathways, thereby increasing the potential for pressure-driven calcium leaching and associated durability degradation in RCC dams (Soysal 2025). This concern is further supported by numerical analyses showing that reservoir-induced hydrodynamic pressure can increase principal tensile stresses and seismic damage demand in RCC dams, thereby increasing the likelihood of crack formation under service-related loading combinations (Şermet et al. 2024).

Most previous studies on calcium leaching focused on diffusion-controlled or immersion-based exposure conditions. Limited attention has been given to calcium leaching under pressure-driven percolation, particularly in HVFA roller-compacted concrete. Although machine-learning models have been successfully used to estimate the compressive strength of cementitious materials from mixture proportions, such models do not directly characterize the residual strength loss caused by pressure-driven chemical degradation (Harirchian 2024). The influence of hydraulic pressure on the coupled evolution of transport behavior, chemical degradation, and mechanical performance remains insufficiently documented. This study examines calcium leaching in HVFA–RCC under different permeation pressures. The objective is to clarify how pressure-driven transport affects calcium loss, microstructural degradation, and strength reduction. The findings aim to provide mechanistic insight that is relevant to durability assessment of RCC dams under long-term service conditions.

2. Experimental Procedure

2.1. Materials

The study used materials similar to the RCC mix design of a large local RCC dam. The mixture compositions consisted of Type I Portland cement in accordance with ASTM C150-90, moderate local calcium fly ash derived from lignite, and fine and coarse basalt aggregates obtained from the nearby borrow pit of the studied RCC dam.

2.1.1. Chemical composition of materials

The chemical compositions of cement, fly ash, and basalt aggregates were determined using an X-ray fluorescence (XRF) spectrometer. The results are presented in Table 1.

Table 1. Chemical compositions of the materials.

Oxides	Composition, %									
	CaO	SiO_2	Al_2O_3	Fe_2O_3	K_2O	Na_2O	MgO	SO_3	NiO	Ignition
Cement	62.67	20.70	4.42	3.07	0.27	0.37	0.91	4.64	2.39	0.56
Fly ash	19.52	31.20	15.59	16.00	1.69	0.03	2.38	9.47	0.01	–
Basalt	6.44	51.28	15.37	9.26	1.63	6.99	2.35	–	–	–

2.1.2. Mix proportions

Three groups of specimens were prepared: paste, mortar, and concrete. Each group was divided into two subgroups: plain cement and cement partially replaced with fly ash at a cement-to-fly ash ratio of 0.9, corresponding to 90 kg/m^3 of cement and 100 kg/m^3 of fly ash. The specimen nomenclature was delineated below: plain cement paste (PC), cement–fly ash paste (PCF), plain cement mortar (MC), cement–fly ash mortar (MCF), plain cement concrete (RC), and fly ash–cement concrete (RCF). Three water-to-binder (w/b) ratios of 0.5, 0.6, and 0.8 were employed, as denoted by the numeral at the commencement of the specimen designation; for instance, 5RCF signifies a concrete mixture incorporating fly ash with a w/b ratio of 0.5. Crushed basalt served as the fine aggregate, exhibiting a fineness modulus (FM) of 3.19, whereas the coarse aggregates were categorized into three groups: G1, G2, and G3, with maximum sizes of 47.25 mm, 31.50 mm, and 16 mm, respectively. Table 2 shows the mix proportion compositions of each specimen type used in this study.

2.1.3. Specimen preparation

Concrete mixes with Vebe times of 75, 60, 55, 50, 45, and 40 seconds, in accordance with ASTM C1170/C1170M, corresponding to specimens 5RC, 5RCF, 6RC, 6RCF, 8RC, and 8RCF, respectively, were cast in cylindrical molds with dimensions of 15 × 30 cm. The specimens were demolded after 24 hours and cured in a water bath at 21 ± 1 °C for 90 days before being subjected to leaching. Cement paste and mortar specimens were cast in short cylindrical molds with dimensions of 15 × 6.40 cm using the same mix compositions as those for the concrete specimens, as shown in Fig. 1.

Table 2. Mix proportions of the specimens.

Specimen	Water/Binder	Cement (kg/m^3)	Fly ash (kg/m^3)	Crushed sand[1] (kg/m^3)	Coarse aggregate[2] (kg/m^3)		
					G1	G2	G3
5PC/5MC[1]/5RC[2]	0.50	190	–	673	568	355	497
6PC/6MC[1]/6RC[2]	0.60	190	–	673	568	355	497
8PC/8MC[1]/8RC[2]	0.80	190	–	673	568	355	497
5PCF/5MCF[1]/5RCF[2]	0.50	90	100	673	568	355	497
5PCF/5MCF[1]/5RCF[2]	0.60	90	100	673	568	355	497
5PCF/5MCF[1]/5RCF[2]	0.80	90	100	673	568	355	497

Note: [1]mortar, [2]concrete

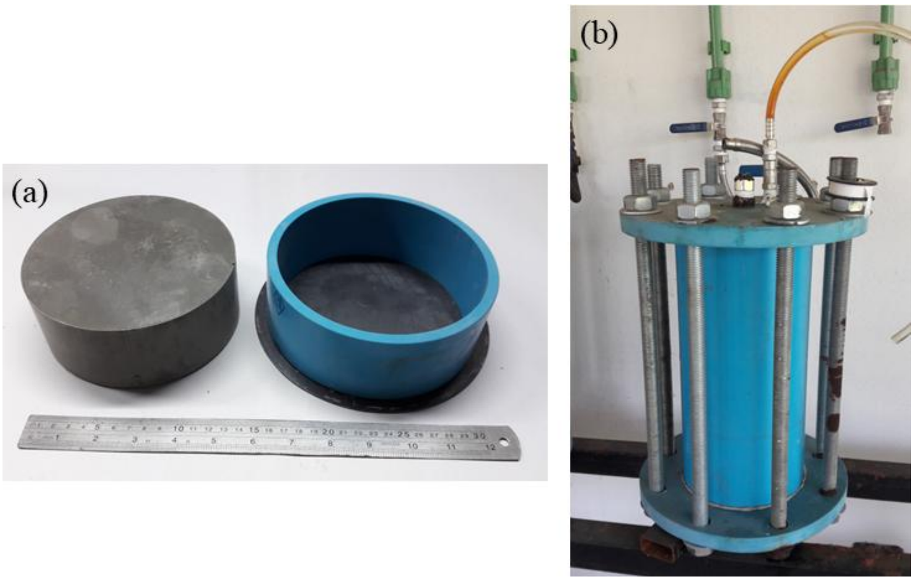

Fig. 1. The shape and size of test specimens: (a) Paste and mortar; (b) RCC.

2.2. Test methods

2.2.1. Accelerated calcium leaching

A 6 M ammonium chloride (NH_4Cl) solution, corresponding to a concentration of 480 g/L, was used to accelerate calcium leaching in this study (Hu et al., 2012). The chemical reactions between ammonium chloride and calcium hydroxide (portlandite, $Ca(OH)_2$) are described in Eqs. (1) and (2).

$$Ca(OH)_2 + 2NH_4Cl \rightarrow CaCl_2 + 2NH_3 + 2H_2O \quad (1)$$

$$CaOSiOH_2O + 2NH_4Cl \rightarrow CaCl_2 + 2NH_3 + SiO_2\,(gel) + H_2O \quad (2)$$

The calcium leaching rate was indirectly assessed by monitoring the pH value of the leaching solution. A decrease in pH reflects the progressive dissolution of calcium-bearing hydration products, particularly calcium hydroxide (CH), which is the most soluble phase during the early stage of leaching. As Ca^{2+} ions are released into the solution, the buffering capacity of the cement matrix is reduced, leading to a measurable decrease in pH. This approach has been widely adopted as an indirect indicator of calcium leaching development in accelerated leaching studies using ammonium chloride solutions (Hu et al. 2012).

2.2.2. Leaching process

A modified percolation leaching apparatus was used to simulate saturated Darcian flow, representing conditions in an RCC dam (Ekström 2003). The specimens were assumed to be isotropic and homogeneous, with randomly distributed pore structures. The test system consisted of a water tank, a high-pressure water pump equipped with a pressure regulator, a piping system, and leaching test cells. Water pressure was applied at 4, 6, and 9 bars to simulate hydraulic heads corresponding to heights of 40, 60, and 90 m, respectively. The leaching tests were conducted for a duration of 28 days. Fig. 2 illustrates the equipment arrangement and leaching setup. Three specimens were tested for each mixture and exposure condition, and the reported values represent average results.

After completion of the leaching procedure, paste and mortar specimens were mechanically cored to obtain cylindrical samples with a diameter of 32 mm and a height of 64 mm for compressive strength testing. Additional sections of each specimen were sectioned into blocks measuring 5 × 5 × 0.5 cm for pore volume determination and microstructural characterization.

Fig. 2. Experimental setup and representative specimens after calcium leaching: (a) Test cell; (b) Percolation apparatus; (c) Leaching process; (d) RCC specimen; (e) Mortar specimen; (f) Sliced paste samples.

2.2.3. Porosity

Three types of specimens—paste, mortar, and concrete—were used for porosity investigation. The pore volume test was conducted in accordance with ASTM C642. After leaching, paste and mortar specimens were cut into pieces measuring 5 × 5 × 0.5 cm. Concrete specimens were cut into disks with a diameter of 150 mm and a thickness of 60 mm for porosity testing.

2.2.4. Microstructure analysis

Microstructural analysis was conducted before and after leaching using scanning electron microscopy (SEM) coupled with energy-dispersive X-ray spectroscopy (EDS). Mineralogical changes induced by leaching were analyzed using X-ray diffraction (XRD). The XRD analysis focused on phase evolution after leaching.

2.2.5. Compressive strength testing

Compressive strength testing was conducted in accordance with ASTM C39 on two types of specimens. The first type consisted of small cylindrical specimens of paste and mortar, with a diameter of 32 mm and a height of 64 mm. The second type consisted of standard concrete specimens, with a diameter of 150 mm and a height of 300 mm.

3. Results and Discussion

Three specimen types—paste, mortar, and concrete—were subjected to leaching for 28 days under applied pressures of 4, 6, and 9 bars. The results are presented below.

3.1. Leaching chemical test

Fig. 3 presents the permeability results of paste and mortar specimens under leaching pressures of 4, 6, and 9 bars. In this study, permeability was used as an indirect indicator of calcium leaching development. Specimens with a water-to-binder ratio (w/b) of 0.8 exhibited the highest permeability for both paste and mortar at all pressure levels. Plain cement paste showed higher permeability than fly ash–cement paste. Plain cement mortar also exhibited higher permeability than fly ash–cement mortar.

At a leaching pressure of 9 bars, permeability reached the highest level. The permeability values at 4 and 6 bars were comparable. Specimens with a w/b ratio of 0.6 showed the lowest permeability at all pressure levels. Mortar specimens exhibited lower permeability than paste specimens, particularly under a leaching pressure of 9 bars. This result indicates a more resistant pore structure in mortar mixtures.

The incorporation of fly ash reduced permeability at all pressure levels. The reduction was more evident at higher water-to-binder ratios and under high pressure. This reduction is attributed to pore-filling effects and pozzolanic reactions. These mechanisms produced a denser cement matrix and improved the interfacial transition zone (ITZ).

The permeability trends are consistent with the porosity results and microstructural observations presented in subsequent sections. This consistency supports the indirect assessment of calcium leaching severity.

The permeability results of concrete specimens under leaching pressures of 6 and 9 bars are shown in Fig. 4. For both fly ash–cement and plain cement concrete, permeability followed a descending order of water-to-binder ratios of 0.8, 0.5, and 0.6.

At a leaching pressure of 9 bars, concrete specimens with w/b ratios of 0.5 and 0.6 exhibited similar permeability values, ranging from approximately 5.2×10^{-9} to 5.6×10^{-9} m/s. These values were lower than those measured for specimens with a higher w/b ratio of 0.8.

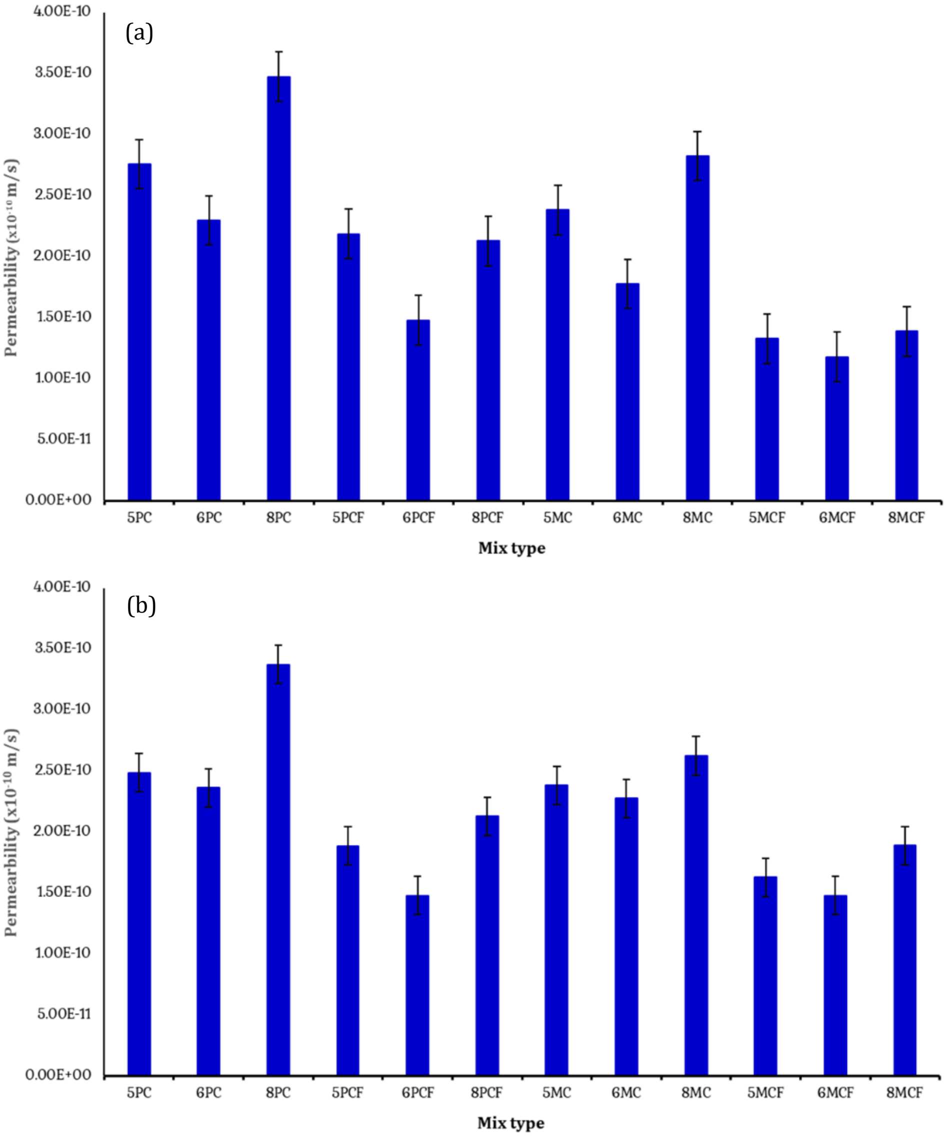

Fig. 3. (continued)

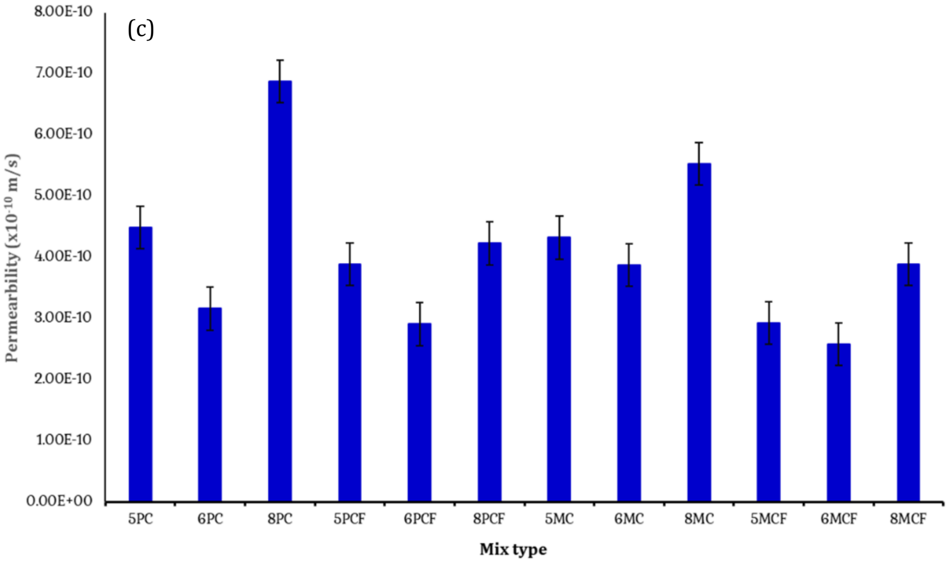

Fig. 3. Average permeability of paste and mortar under different pressure: (a) 4 bars; (b) 6 bars; (c) 9 bars.

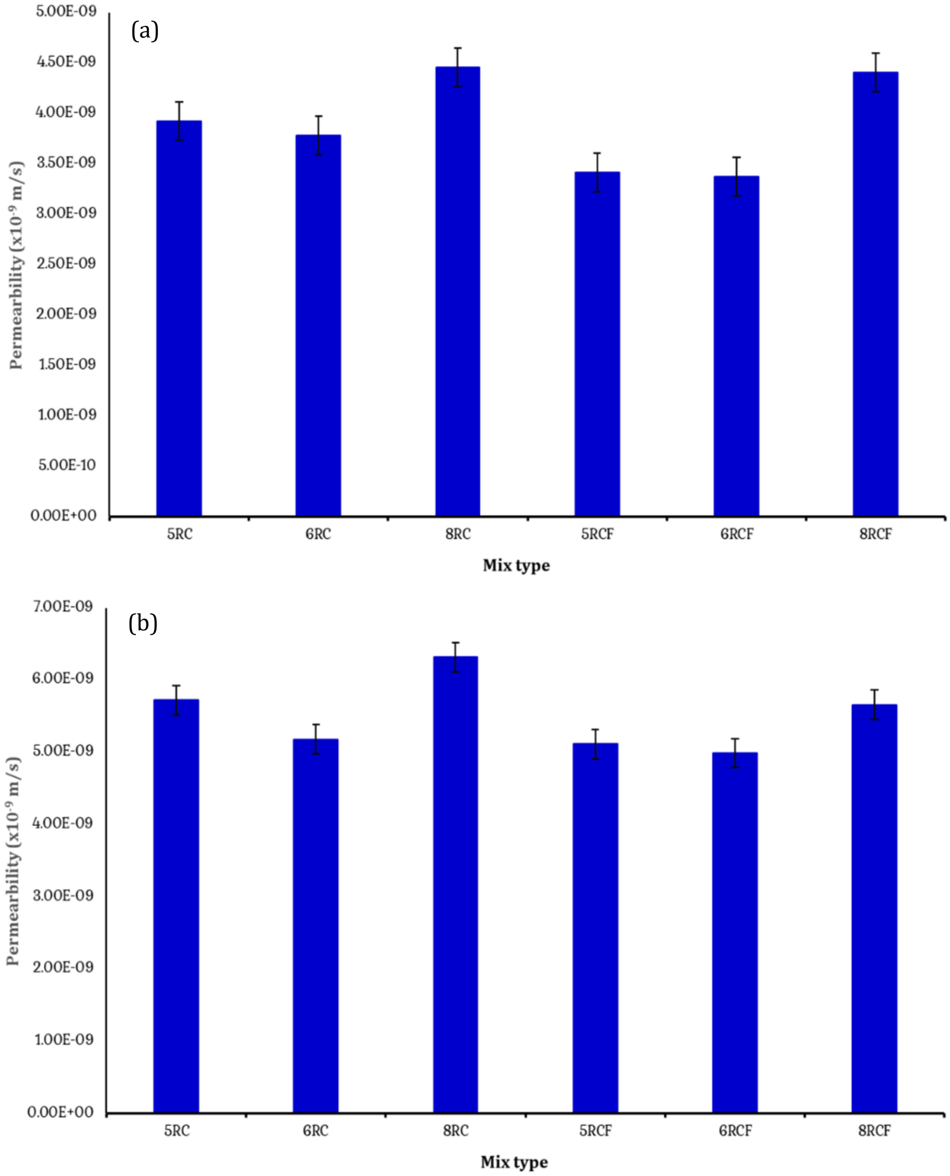

Fig. 4. Permeability of concrete specimens under high pressure: (a) 6 bars; (b) 9 bars.

3.2. Porosity

The porosity characteristics of paste specimens after calcium leaching are shown in Fig. 5. Calcium leaching increased the volume of voids (%) in all specimens. The extent of the increase depended on leaching pressure and water-to-binder ratio.

At a leaching pressure of 4 bars, the volume of voids (%) increased slightly. Specimens with low water-to-binder ratios (w/b = 0.5 and 0.6) showed an increase in void volume of approximately 14–16%. Specimens with a higher water-to-binder ratio (w/b = 0.8) showed a larger increase in void volume.

At a leaching pressure of 6 bars, the volume of voids (%) increased further in all mixtures. The increase ranged from 14–18% for specimens with lower w/b ratios. Specimens with a w/b ratio of 0.8 showed an increase in void volume of up to approximately 20%.

At a leaching pressure of 9 bars, the void volume (%) reached the highest level. All specimens showed a substantial increase in void volume. The increase was more pronounced in specimens with higher water-to-binder ratios. This reflects severe degradation of the cement matrix under high permeation pressure.

The porosity results confirm that both leaching pressure and water-to-binder ratio govern pore structure development. Higher leaching pressure increased calcium dissolution. A higher w/b ratio increased void volume and pore connectivity.

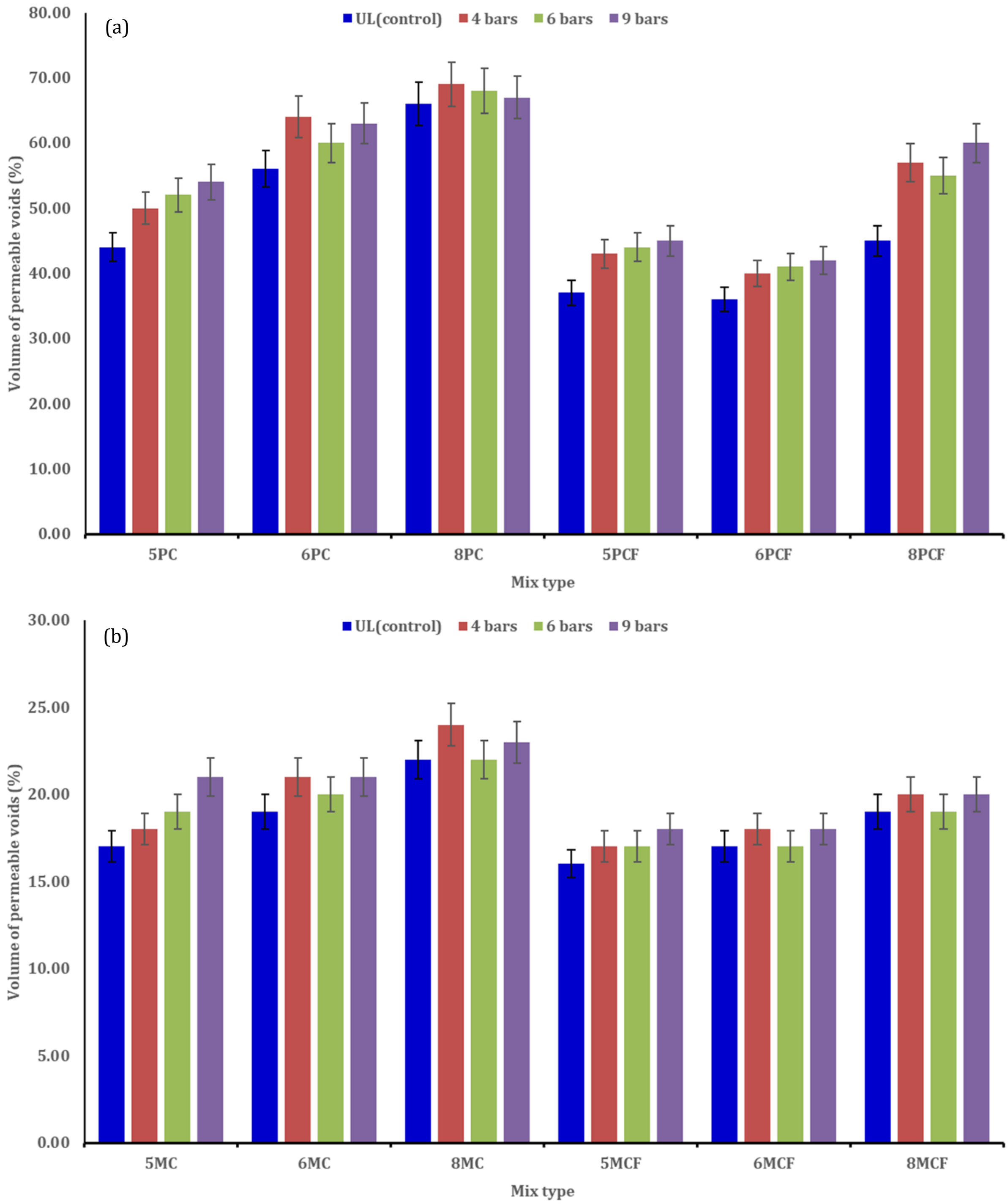

Fig. 5. (continued)

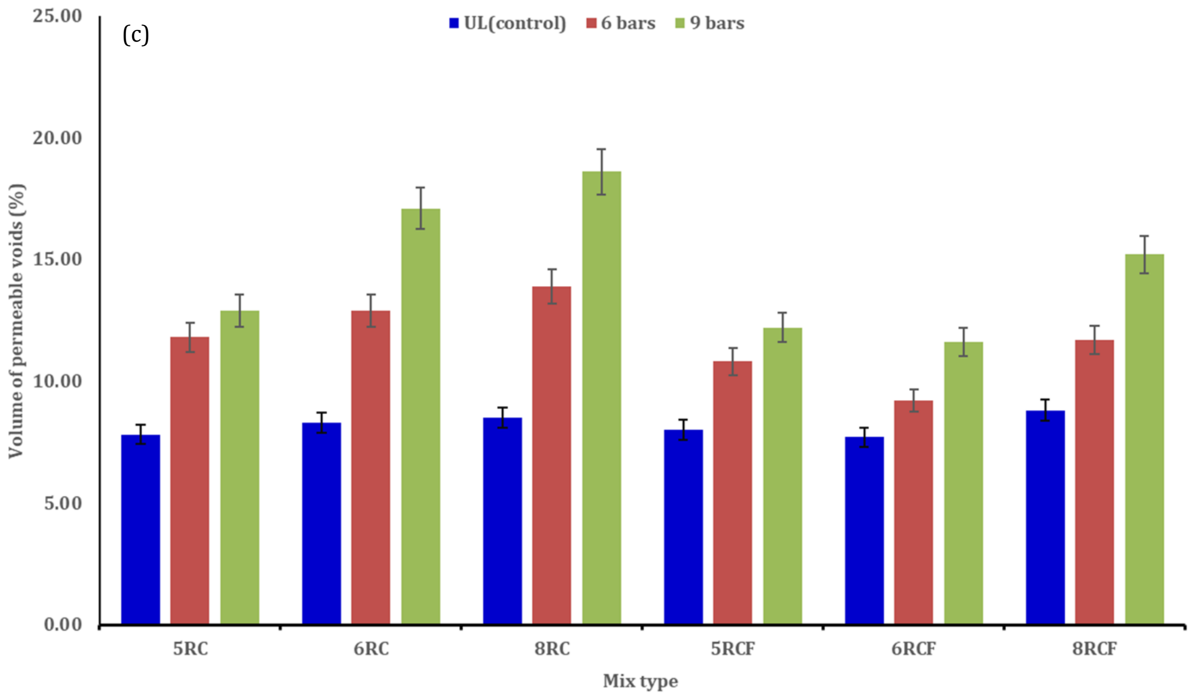

Fig. 5. The relationship of pore volume and applied leaching pressure: (a) Paste; (b) Mortar; (c) RCC.

3.3. Microstructural analysis

The microstructural characteristics of the paste specimens after calcium leaching were examined using SEM, as shown in Fig. 6. The SEM images illustrate comparative microstructural trends caused by calcium leaching. They are not intended to provide quantitative measurements of pore structure. The unleached specimens show a dense and continuous hydration matrix. Abundant C–S–H gel and well-distributed crystalline phases occupy the binder. In contrast, the leached specimens show clear degradation. Porosity increases, and microcracks become visible.

At a leaching pressure of 4 bars, the microstructure remains relatively compact. Specimens with low water-to-binder ratios (w/b = 0.5 and 0.6) show limited dissolution of calcium hydroxide. The C–S–H framework remains largely preserved, and microcracks are rare. Specimens with a higher w/b ratio (w/b = 0.8) contain small voids, but the matrix still maintains overall continuity. At a leaching pressure of 6 bars, microstructural damage becomes more evident. Voids and microcracks increase in all mixtures. Specimens with lower w/b ratios retain a partially connected C–S–H structure. Specimens with a higher w/b ratio exhibit a less dense and more fragmented matrix. Enlarged pores and localized cracking become more pronounced as w/b increases. At a leaching pressure of 9 bars, severe degradation occurs. Extensive voids and connected crack networks appear in all specimens. Damage remains limited in mixtures with low w/b ratios, but it becomes severe in the specimen with w/b = 0.8. In this case, the cement matrix appears highly porous and discontinuous.

Microstructural deterioration increases with both leaching pressure and water-to-binder ratio. At lower pressure, dissolution mainly affects localized regions of the matrix. At higher pressure and higher w/b ratios, calcium dissolution becomes widespread. This process accelerates pore connectivity and leads to a significant loss of structural integrity. These observations link directly to changes in the Ca/Si ratio of the C–S–H gel. In the unleached state, portlandite acts as a calcium reservoir and stabilizes the hydration system. Calcium leaching first dissolves portlandite, and this reduces calcium concentration in the pore solution. The equilibrium then shifts, and calcium begins to extract from the C–S–H gel. The Ca/Si ratio decreases, and the gel undergoes decalcification. The gel contracts, loses cohesion, and becomes more porous. This chemical transformation appears in the SEM images as gel fragmentation and pore opening.

The rate of Ca/Si reduction depends strongly on the initial pore structure. Low w/b mixtures restrict calcium transport and slow the decalcification process. High w/b mixtures contain interconnected pore networks that accelerate ion migration. As a result, the Ca/Si ratio drops throughout the matrix, and structural breakdown spreads rapidly. The SEM damage patterns therefore represent a direct microstructural expression of Ca/Si evolution in the binder phase. As the Ca/Si ratio decreases, the load-bearing capacity of the C–S–H gel declines, and the matrix transitions from a cohesive framework to a porous skeletal structure.

The calcium ion analysis obtained from EDS is shown in Fig. 7 At a low applied pressure of 4 bars, the percentage decrease of Ca^{2+} relative to the unleached specimens was 8%, 4%, and 8% for 5PCF, 6PCF, and 8PCF, respectively. At a moderate applied pressure of 6 bars, the Ca^{2+} reduction increased to 27%, 10%, and 45%. At a high applied pressure of 9 bars, the corresponding reductions further increased to 42%, 29%, and 50%.

The results indicate that Ca^{2+} leaching increased with applied pressure. The effect was more pronounced in specimens with higher water-to-binder ratios. This behavior suggests that pressure-induced microstructural changes enhanced calcium leaching in high w/b specimens compared with those with lower w/b ratios.

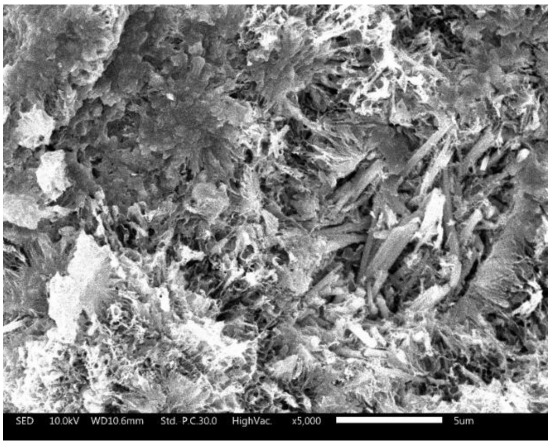

5 bar PCF-UL

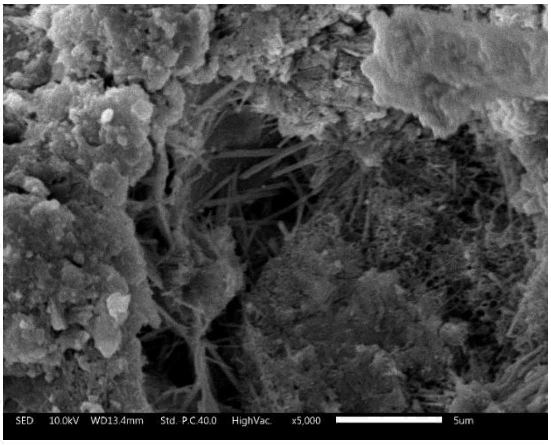

4 bar 5PCF

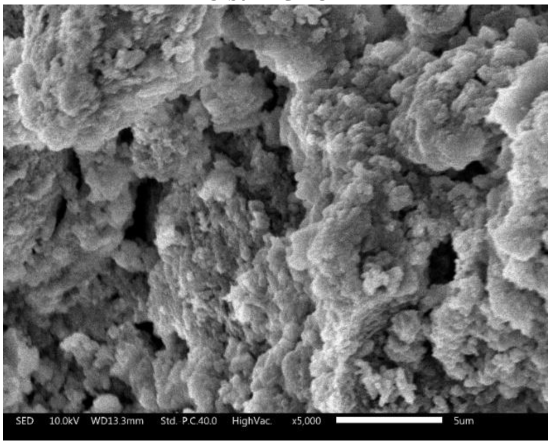

6 bar 5PCF

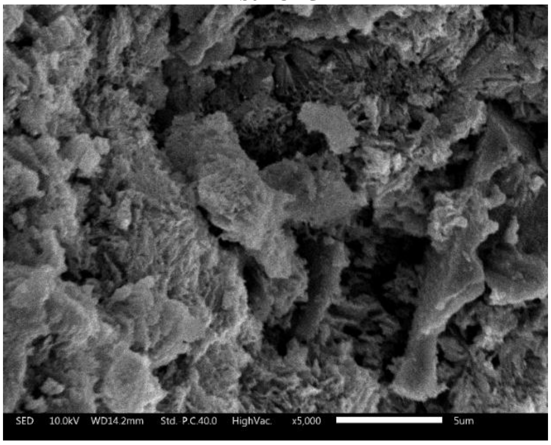

9 bar 5PCF

(a) w/b = 0.5

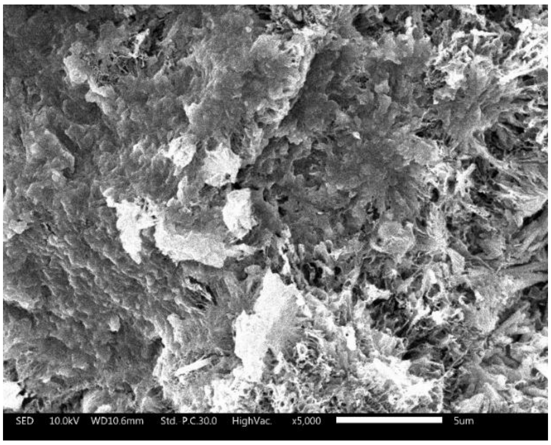

6 bar PCF-UL

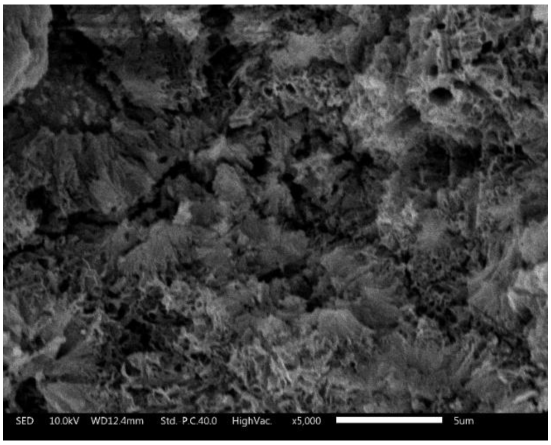

4 bar 6PCF

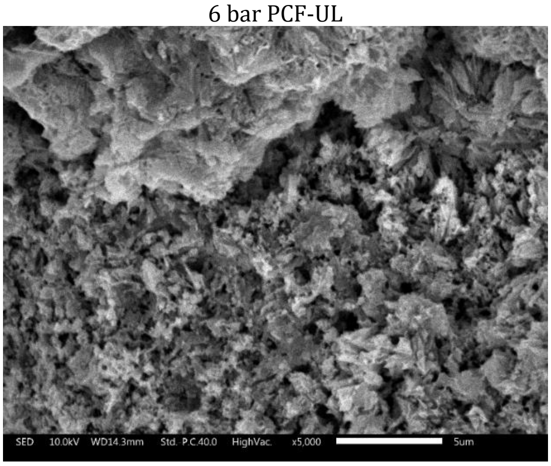

6 bar 6PCF

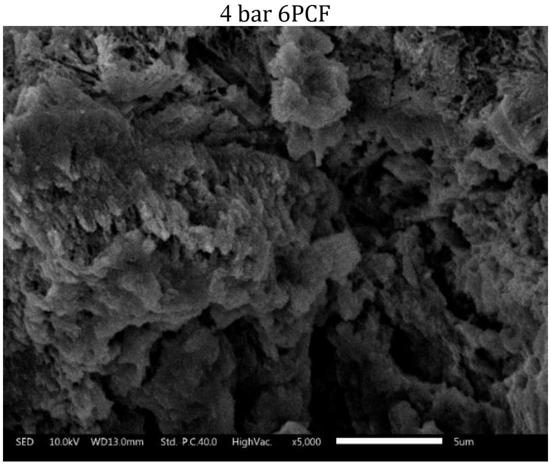

9 bar 6PCF

(b) w/b = 0.6

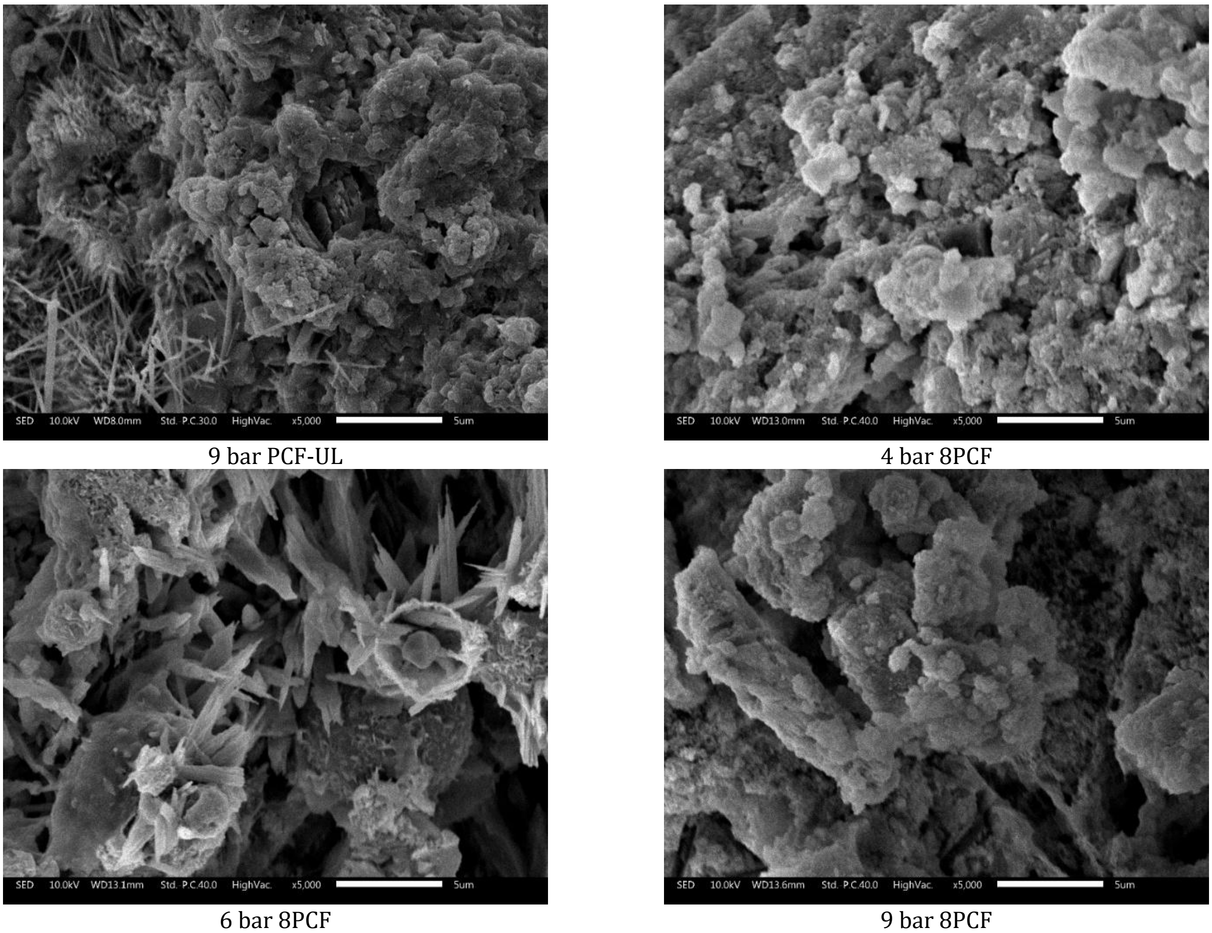

(c) w/b = 0.8

Fig. 6. The microstructure of the paste (w/b = 0.5, 0.6, and 0.8) under pressure of 4, 6, and 9 bars.

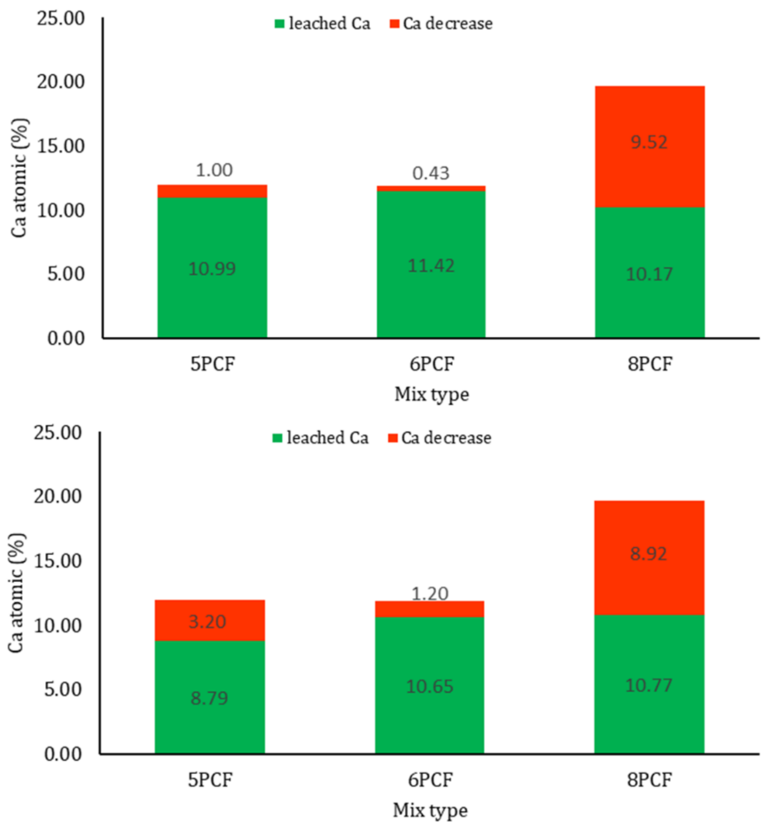

Fig. 7. (continued)

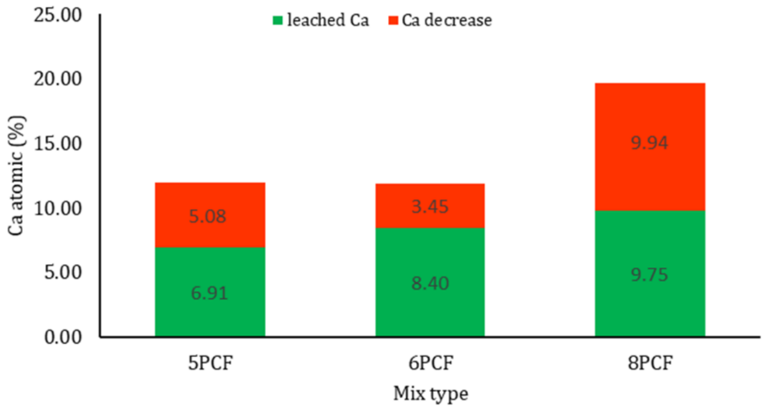

Fig. 7. The results of SEM/EDS of calcium leaching from pastes under pressure: (a) 4 bars; (b) 6 bars; (c) 9 bars.

The leaching results obtained from XRD analysis are presented in Fig. 8. The figure shows differences in calcium-bearing phases of fly ash–cement paste between unleached and leached specimens under different pressures. A significant reduction in the intensity of the portlandite (CH) peak was observed in the leached specimens. A slight reduction in the C–S–H-related peak was also detected.

The reduction in CH peak intensity increased with applied pressure. Specimens with a water-to-binder ratio of 0.8 exhibited the largest decrease in CH intensity. This result indicates that high w/b specimens were more strongly affected by the leaching process. This microstructural deterioration corresponds well with the observed increase in porosity and pore connectivity under pressure-driven leaching conditions. These changes directly explain the reduction in compressive strength reported in the subsequent section.

In this study, transport behavior was not measured directly using permeability or diffusion coefficients. Instead, it was inferred from permeability trends, porosity evolution, and microstructural features such as pore connectivity and cracking. These indicators collectively reflect changes in transport pathways governing pressure-driven calcium leaching.

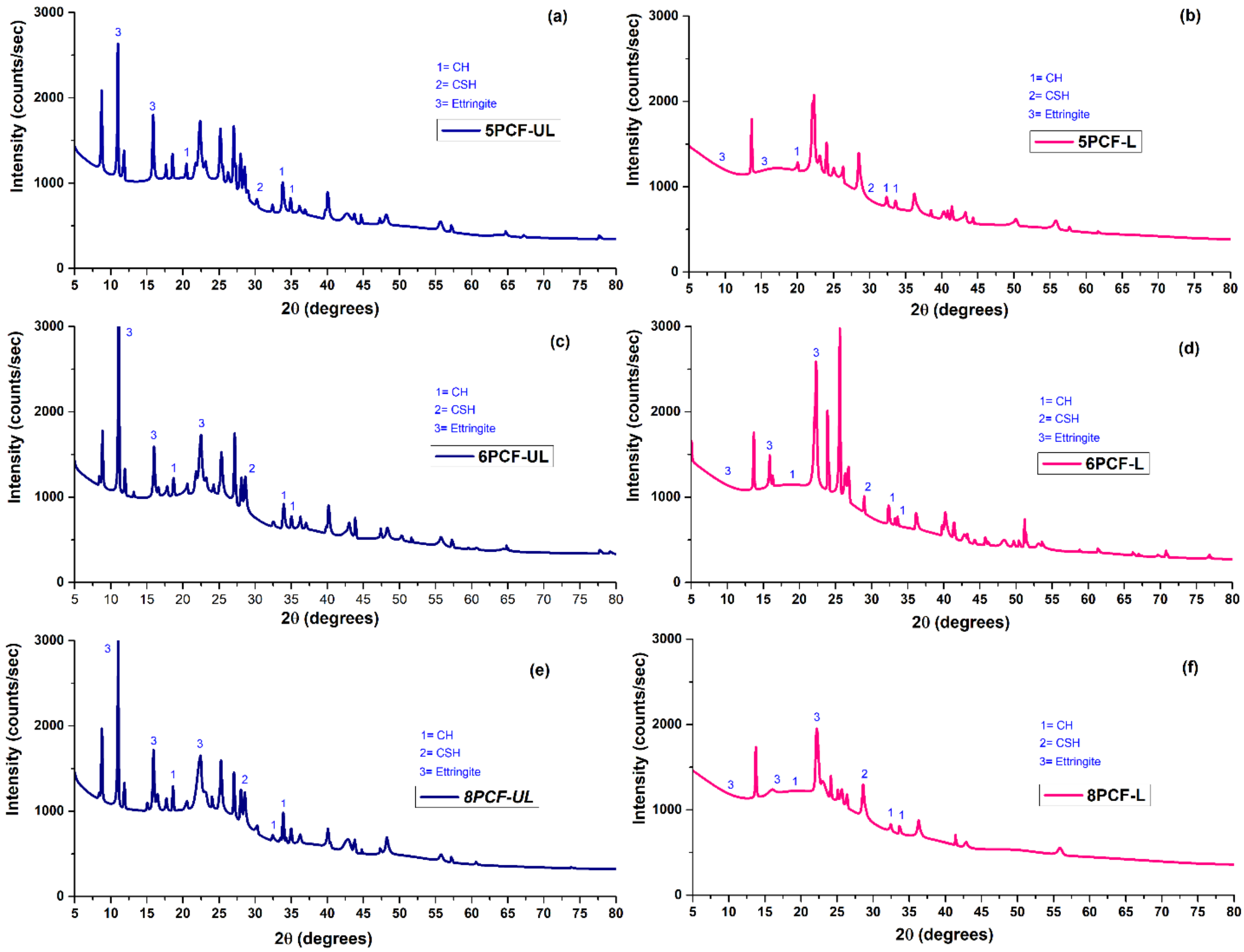

Fig. 8. The results of XRD fly ash cement pastes, unleached condition, and leached condition under pressure of 6 bars.

3.4. Compressive strength

The observed strength degradation can therefore be interpreted as a direct consequence of calcium leaching–induced microstructural weakening, including pore coarsening and degradation of the ITZ. The compressive strengths of leached paste specimens are presented in Fig. 9. For water-to-binder (w/b) ratios of 0.5 and 0.6, the plain cement paste exhibited higher compressive strength than the corresponding fly ash–cement paste, whereas a slight increase in compressive strength was observed for both paste types at a w/b ratio of 0.8. Leaching under pressures of 4, 6, and 9 bars reduced the compressive strength of plain cement paste by approximately 28–31%, 37–74%, and 49–79%, respectively. For fly ash–cement paste specimens, the corresponding strength reductions were about 43–60%, 49–62%, and 47–61% relative to the unleached specimens. Although higher leaching pressure resulted in greater compressive strength loss, with the reduction being more pronounced at 9 bars than at 6 bars, the effect at 4 bars was comparatively limited.

The dissolution of calcium-bearing hydration products occurs during the leaching process. This process weakens the cement matrix and leads to a decrease in compressive strength. A smaller strength reduction was observed at lower pressure, while higher pressure resulted in more pronounced strength loss. The more pronounced strength loss at higher pressures indicates increased leaching intensity. Under certain conditions, plain cement paste exhibited slightly higher compressive strength than fly ash–cement paste. This behavior can be attributed to the higher initial calcium hydroxide content available before leaching.

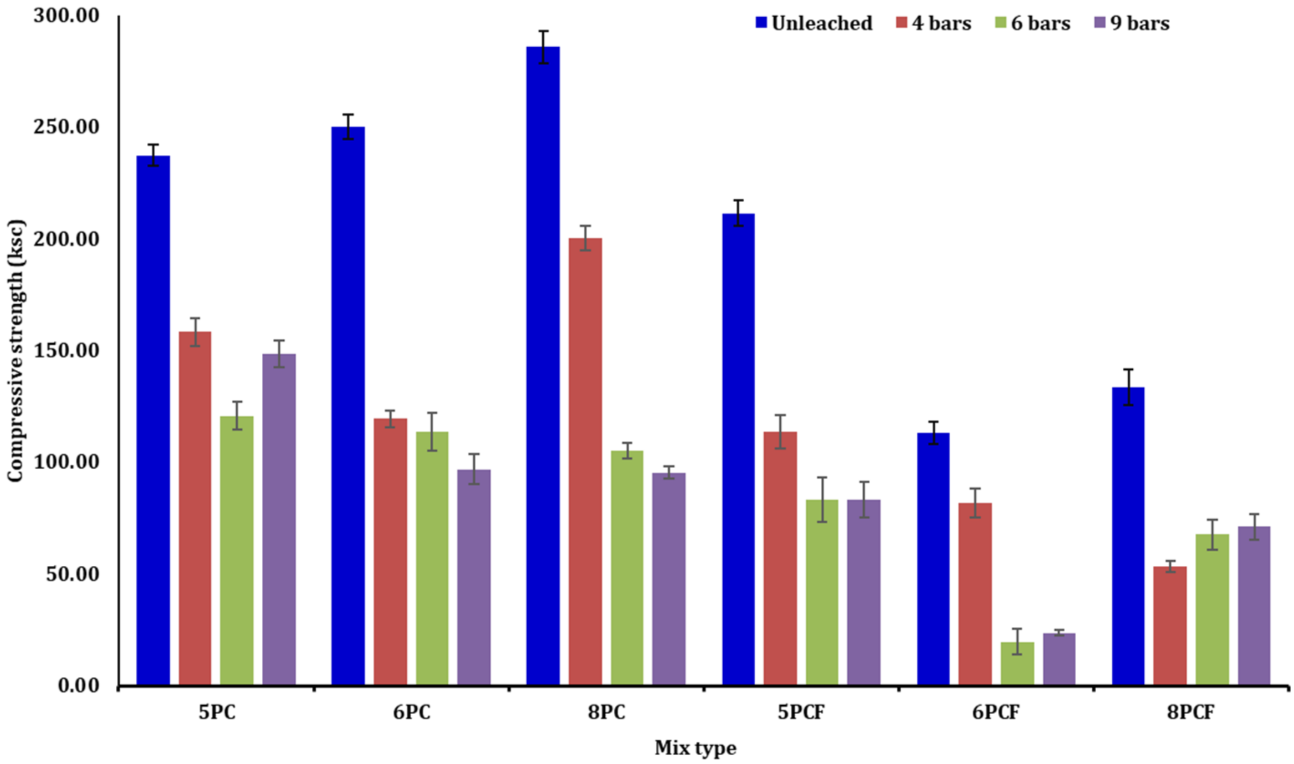

Fig. 9. Compressive strength and leaching pressure relationship of pastes.

For mortar specimens, the effects of calcium leaching on compressive strength are shown in Fig. 10. Under leaching pressures of 4, 6, and 9 bars, the compressive strength of plain cement mortar decreased by approximately 5–12%, 10–13%, and 24–43%, respectively. For fly ash–cement mortar, the corresponding reductions were about 4–16%, 7–22%, and 14–28%. Overall, greater leaching pressure resulted in larger compressive strength loss.

Higher leaching pressure caused greater compressive strength loss in the mortar specimens. At low pressure, leaching mainly occurred through percolation. Diffusion effects became more evident as pressure increased (Torrenti et al. 2008). The influence of fly ash under the same pressure level depended on the water-to-binder ratio. Strength reductions of approximately 2–29% were observed at w/b ratios of 0.5 and 0.6. Mortars with higher w/b ratios showed lower compressive strength. This behavior was related to changes in the fine aggregate-to-binder ratio and increased porosity. The pozzolanic reaction refined the pore structure. However, leaching-induced damage in the interfacial transition zone (ITZ) led to additional strength loss (Galle et al. 2008).

The compressive strength results of the concrete specimens are shown in Fig. 11. Calcium leaching reduced the compressive strength of concrete, and the strength loss increased with permeation pressure. Fly ash–cement concrete showed relatively small strength reductions of about 5–15% and 5–19% under leaching pressures of 6 and 9 bars, respectively, compared to the unleached specimens. At a high water-to-binder ratio (w/b=0.8), the compressive strength dropped to about 133 kg/cm^2. This corresponds to a strength reduction of approximately 37–54%.

Calcium leaching reduced the compressive strength of concrete under permeation pressure. This strength loss was associated with damage to the concrete microstructure. Fly ash–cement concrete showed a smaller strength reduction than plain cement concrete. At high water-to-binder ratios, increased porosity made the concrete more vulnerable to leaching. This led to severe strength loss. The use of fly ash reduced calcium hydroxide content and refined the pore structure through pozzolanic reactions. As a result, HVFA-RCC exhibited better resistance to calcium leaching when an appropriate binder composition and w/b ratio were used.

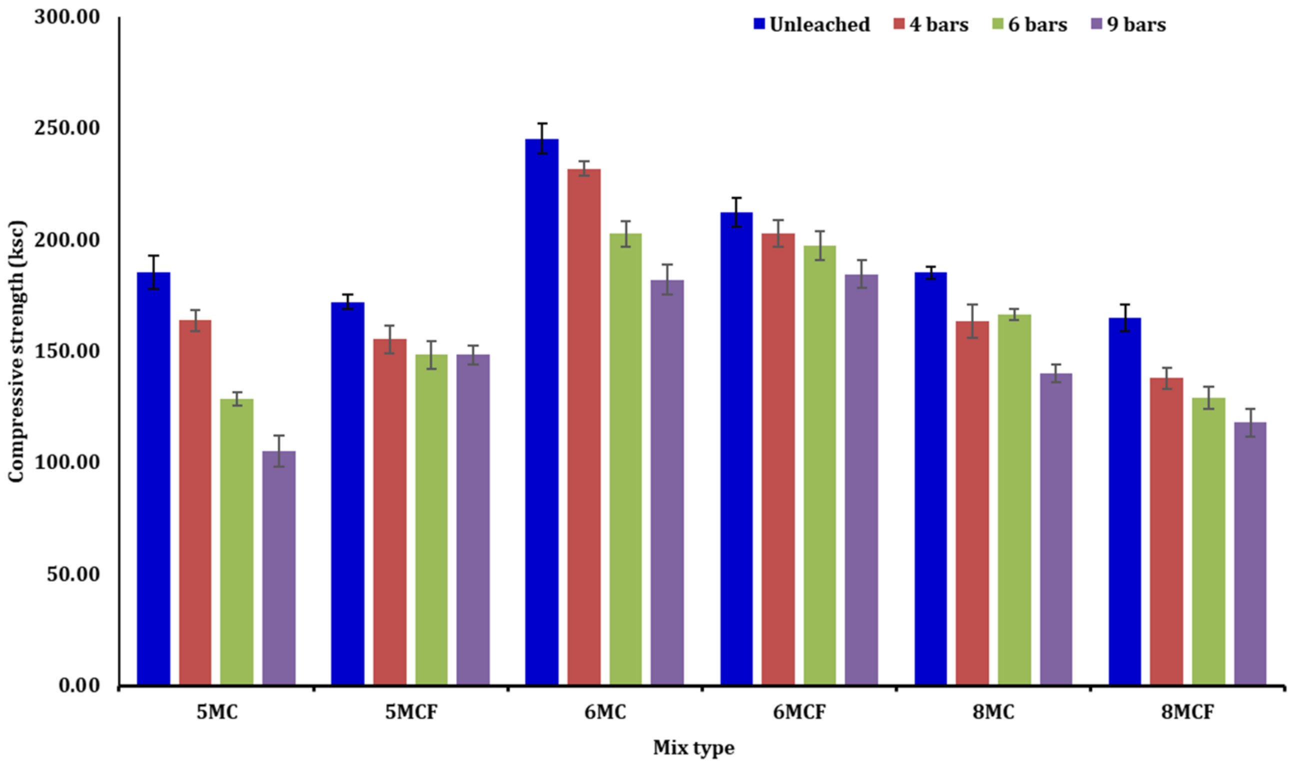

Fig. 10. Compressive strength and leaching pressure relationship of mortars.

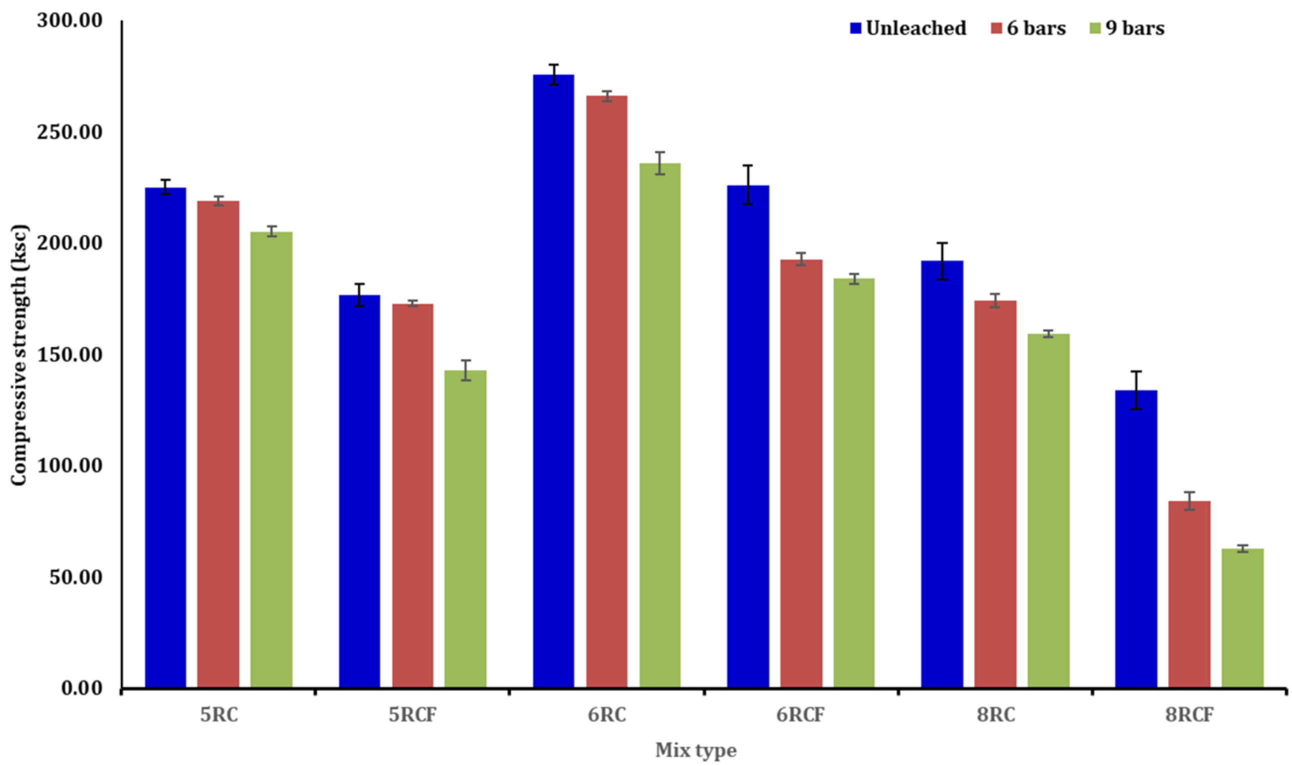

Fig. 11. Compressive strength and leaching pressure relationship of RCC.

4. Conclusions

This study presents a mechanistic evaluation of calcium leaching in high-volume fly ash roller-compacted concrete (HVFA-RCC) under pressure-driven permeation, with direct relevance to hydraulic structures such as RCC dams. The results show that calcium leaching in HVFA-RCC is controlled by the combined effects of chemical degradation and transport processes. This coupled behavior differs from diffusion-dominated or immersion-based leaching mechanisms commonly reported in previous studies. Pressure-driven permeation introduces an additional transport component. This component alters the progression of calcium loss. As a result, the governing leaching mechanisms are fundamentally different.

From a chemical perspective, HVFA-RCC contains a lower initial amount of portlandite and undergoes continued pozzolanic consumption of calcium hydroxide. These processes modify the chemistry of C–S–H toward lower Ca/Si ratios and improved phase stability. Calcium depletion from the cement matrix occurs at a slower rate. Microstructural degradation is less severe than in plain cement systems. Accordingly, HVFA-RCC shows smaller increases in porosity. These effects are directly associated with fly ash. Fly ash reduces portlandite availability, refines pore structure, and stabilizes the C–S–H phase under leaching conditions. Compressive strength loss is also reduced under identical permeation conditions.

From a transport standpoint, permeation pressure plays a key role in accelerating calcium leaching. Higher pressure enhances advective transport through connected pore networks. Calcium removal increases due to pressure-driven flow in addition to diffusion. Chemical decalcification intensifies as a result. Microstructural damage becomes more pronounced. This effect is especially evident in mixtures with higher water-to-binder ratios, where pore connectivity is greater. Mechanical degradation consistently follows both chemical decalcification and pressure-controlled transport intensity.

In RCC dams, continuous seepage and hydraulic pressure gradients develop along the dam height. Regions exposed to higher pressures are, therefore, more vulnerable to accelerated calcium leaching. Durability loss becomes more pronounced under these conditions. The incorporation of high-volume fly ash reduces the sensitivity of RCC to pressure-induced leaching. This behavior provides a durability advantage over plain cement systems.

Several limitations should be acknowledged. The accelerated NH_4Cl leaching method was employed to shorten the experimental duration and to promote controlled decalcification. However, this approach does not reproduce the chemical composition or timescale of natural seepage conditions, and the findings should therefore be interpreted in a mechanistic and comparative context. It differs from natural seepage water in RCC dams. Direct measurements of calcium flux were not conducted. The results should therefore be interpreted as a comparative and mechanistic assessment. Direct prediction of field leaching rates is not intended. Future studies should include direct calcium measurements and long-term exposure conditions. These efforts will further refine service-life evaluations of HVFA-RCC dams.

Acknowledgements
None declared.

Funding
The authors received no financial support for the research, authorship, and/or publication of this manuscript.

Conflict of Interest
The authors declare no potential conflicts of interest with respect to the research, authorship, and/or publication of this manuscript.

Data Availability
The datasets generated and/or analyzed during the current study are not publicly available but are available from the corresponding author upon reasonable request.

AI Assistance
No AI-based tools were used in the preparation of this manuscript.

Author Contributions
All authors made substantial contributions to the conception and design of the study, acquisition of data, analysis and interpretation of data; drafted or critically revised the manuscript for important intellectual content; and approved the final version to be published.

References

Al-Safi S, Altharehi A, Alameri IA, Al-Jolahy A (2025). The mechanical properties of cement mortar reinforced with silica fume subjected to sulfate and chloride environment. *Challenge Journal of Structural Mechanics*, 11(1), 55-69.

ASTM C39 (2004). Standard test method for compressive strength of cylindrical concrete specimens. ASTM International, West Conshohocken, PA, USA.

ASTM C136 (2005). Standard test method for sieve analysis of fine and coarse aggregates. ASTM International, West Conshohocken, PA, USA.

ASTM C150 (1990). Standard specification for Portland cement. ASTM International, West Conshohocken, PA, USA.

ASTM C470 (2000). Standard specification for molds for forming concrete test cylinders vertically. ASTM International, West Conshohocken, PA, USA.

ASTM C642 (1997). Standard test method for density, absorption, and voids in hardened concrete. ASTM International, West Conshohocken, PA, USA.

ASTM C1170 (1998). Standard test methods for determining consistency and density of roller compacted concrete using a vibrating table. ASTM International, West Conshohocken, PA, USA.

Bache HH, Idorn GM, Nepper-Christensen P, Nielsen J (1966). Morphology of calcium hydroxide in cement paste. *Proceedings of the Symposium on Structure of Portland Cement Paste and Concrete*, Washington, D.C., USA, 154-174.

Carde C, François R (1997). Effect of the leaching of calcium hydroxide from cement paste on mechanical and physical properties. *Cement and Concrete Research*, 27(4), 539-550.

Chaisiwamongcol N (2008). Behaviors of Khun Dan Prakarnchon Dam During Construction and Initial Impounding. *M.Sc. thesis*, Kasetsart University, Bangkok, Thailand. (in Thai)

Chen X, Zhou M, Liu J, Wang Y (2023). Coupled transport-chemical degradation of cement-based materials under pressure-driven flow. *Cement and Concrete Composites*, 137, 104889.

Cheng A, Chao SJ, Lin WT (2013). Effects of leaching behavior of calcium ions on compression and durability of cement-based materials with mineral admixtures. *Materials*, 6(5), 1851-1872.

Choi YS, Yang EI (2013). Effect of calcium leaching on the pore structure, strength, and chloride penetration resistance in concrete specimens. *Nuclear Engineering and Design*, 259, 126-136.

Ekström T (2003). The Leaching Process and Its Effects. *Ph.D. thesis*, Lund University, Lund, Sweden.

Fanghui H, Rengguang L, Peiyu Y (2014). Effect of freshwater leaching on the microstructure of hardened composite binder pastes. *Construction and Building Materials*, 68, 630-636.

Galle C, Peycelon H, Le Bescop P (2008). Effect of accelerated chemical degradation on water permeability. *Cement and Concrete Research*, 38(4), 455-469.

Harirchian E (2024). Predicting compressive strength of AAC blocks through machine learning advancements. *Challenge Journal of Concrete Research Letters*, 15(2), 56-68.

Hu Y, Jiang L, Zhang Y, Pu Q, Xu Y (2012). Predicting the calcium leaching behavior of cement pastes in aggressive environments. *Construction and Building Materials*, 29, 88-96.

Inmala N, Soralump S (2010). Safety analysis of RCC dam from seepage through dam model case study. *Proceedings of the 15th National Convention on Civil Engineering*, Ubon Ratchathani, Thailand.

Kadhim AL, Keskin SB (2024). Calcium aluminate cement based high early strength engineered cementitious composites with recycled artificial flaws. *Challenge Journal of Concrete Research Letters*, 15(4), 120-133.

Lin L, Wang X, Zhou J, Chu H, Shen D, Chen H, Qin S (2018). Investigation of pore structure and mechanical property of cement paste subjected to the coupled action of freezing/thawing and calcium leaching. *Cement and Concrete Research*, 109, 133-146.

Liu J, Zhang Y, Wang Y, Jiang L (2022). Transport properties and calcium leaching of cementitious materials under seepage conditions. *Construction and Building Materials*, 318, 125960.

Mahmud H, Ahmed T, Islam MS (2025). Combined effect of rice husk ash and animal bone powder on strength and permeability of concrete. *Challenge Journal of Structural Mechanics*, 11(1), 1-13.

Marchand J, Bentz D, Samson E, Maltais Y (2001). Influence of calcium hydroxide dissolution on the transport properties of hydrated cement systems. In: Skalny JP, Gebauer J, Odler I, editors. *Materials Science of Concrete: Calcium Hydroxide in Concrete*. American Ceramic Society, Westerville, OH, USA, 113-129.

Mindess S, Young JF, Darwin D (2003). Concrete. 2nd ed. Pearson Education Inc., Upper Saddle River, NJ, USA.

Pandimani (2025). Assessment of stresses and vibration behavior of concrete gravity dam under fluctuating hydrostatic force. *Challenge Journal of Concrete Research Letters*, 16(1), 1-14.

Rozière E, Loukili A, El Hachem R, Grondin F (2009). Durability of concrete exposed to leaching and external sulfate attacks. *Cement and Concrete Research*, 39, 1188-1198.

Şermet F, Kartal ME, Yiğit ME, Hökelekli E (2024). The effect of the gravity on the earthquake performance of roller compacted concrete dams. *Challenge Journal of Concrete Research Letters*, 15(1), 20-29.

Shaheen YBI, Etman ZA, Sabiha HL (2025). Design of reactive powder concrete mortar mixes through high strength and durability. *Challenge Journal of Concrete Research Letters*, 16(3), 142-154.

Shi C, Wang D, Wu Z, Wu L (2019). Calcium leaching behavior of cementitious materials with supplementary cementitious materials. *Construction and Building Materials*, 221, 196-206.

Soysal BF (2025). A discrete element method for evaluating the seismic performance of concrete gravity dam-reservoir systems under main shock-aftershock events. *Challenge Journal of Structural Mechanics*, 11(4), 229-244.

Torrenti JM, Nguyen VH, Colina H, Le Maou F, Benboudjema F, Deleruyelle F (2008). Coupling between leaching and creep of concrete. *Cement and Concrete Research*, 38(6), 816-821.

Turan E, Alameri IA, Oltulu M (2025). Long-term durability of red mud-modified cement mortars: Effects of high temperature and freeze-thaw cycles. *Challenge Journal of Structural Mechanics*, 11(3), 116-127.

Wang Y, Liu J, Zhang J, Jiang L (2021). Effect of fly ash on calcium leaching properties of cement pastes in ammonium chloride solution. *Materials*, 14(19), 5935.

Zhang Y, Liu Z, Jiang Y, Guo L, Song Z (2020). Determination of calcium leaching behavior of cement pastes exposed to ammonium chloride aqueous solution. *Cement and Concrete Research*, 134, 106086.